## PAPER

Check for updates

# Green synthesis of glucose-capped stable silver nanoparticles: a cost-effective sensor for the selective detection of Hg$^{2+}$ ions in aqueous solutions

Chinmayee Pattnaik,[ab] Ritisnigdha Mishra,[a] Ashok K. Sahu,[bc] Laxmi Narayan Sahoo,[bd] Naba K. Sahoo,[b] Sukanta Kumar Tripathy*[bc] and Satyanarayan Sahoo (iD) *[ab]

We, herein, report a unique, cost-efficient, and green method for the synthesis of glucose-capped silver nanoparticles (AgNPs) using *Ocimum sanctum* (tulsi) leaf extract for the detection of Hg$^{2+}$ ions in water. The nanoparticles synthesized by the above-mentioned method were found to be highly stable. The higher stability of the glucose-capped nanoparticles may be due to the interaction of hydroxyl groups of carbohydrate molecules with the nanoparticles. The optical and structural properties of the nanoparticles were confirmed by different spectroscopic methods. The selective detection of Hg$^{2+}$ ions by the AgNPs was studied by colorimetric analysis and optical absorption spectroscopy. The detection of Hg$^{2+}$ ions was also investigated by fabricating an optical fiber using AgNPs. From the optical fiber-based experiments, the limit of detection (LOD) for Hg$^{2+}$ ions using the sugar-capped AgNPs was found to be 2.8 ppb, which is better than that of many other sensors based on green AgNPs reported in the literature. The improvement in the value of LOD with sugar-capped AgNPs showed the impact of carbohydrates on the sensing abilities of AgNPs. The sensing ability of the AgNPs for Hg$^{2+}$ ions was further verified by a nanoparticle-coated filter paper strip method.

## 1. Introduction

The rapid development in science and technology is associated with large-scale environmental contamination. The contaminants are mainly heavy metals that have several negative consequences on the environment, human beings, and aquatic life. Heavy metals accumulate in numerous body parts and are hazardous to human health because they are non-biodegradable and have longer biological half-lives. Some of the heavy metals are toxic because of their higher water solubility. Among the various heavy metals such as Cd$^{2+}$, Pb$^{2+}$, As$^{3+}$, Cr$^{2+}$, and Hg$^{2+}$, the Hg$^{2+}$ ion, as a pollutant, has received a lot of concern due to the carcinogenic effect on the aqueous environment.[1] Mercury is released into the environment as an industrial waste from gold mining, gasoline additives, and petrol refining industries.[2,3] It exists in three forms such as elemental (or metallic) mercury, inorganic mercury, and organic mercury, all of which are toxic to various living animals. As a non-biodegradable metal, mercury is liberated into the aquatic environment, mainly in the inorganic form. Even a low concentration of mercury can have an adverse effect on marine flora and fauna. It is observed from various studies that mercury accumulates in several body parts such as the brain, liver, and kidney through the food chain and can damage the gastrointestinal tract, epidermal tissue, renal tissue, and nervous system.[4,5] Bacterial species in water bodies convert water-soluble divalent mercuric ions (Hg$^{2+}$) into organic mercuric compounds such as ethylmercury (EtHg$^{+}$) and methylmercury (MeHg$^{+}$).[6] Methylmercury is highly toxic, as compared to inorganic mercury, as it is a dominant neurotoxin and causes significant health issues such as motor and sensory nerve damage.[7–9] It also binds with haemoglobin which acts as a carrier of methylmercury in blood to different organs. Methylmercury is absorbed more readily by the body and is excreted more slowly than other forms of mercury.

[a] *P. G. Department of Chemistry, Berhampur University, Odisha, 760007, India. E-mail: sns.chem@buodisha.edu.in*
[b] *Centre of Excellence in Nanoscience and Technology for the Development of Sensor, Berhampur University, Odisha, 760007, India. E-mail: skt.phy@buodisha.edu.in*
[c] *P. G. Department of Physics, Berhampur University, Odisha, 760007, India*
[d] *Department of Chemistry, Government Science College Chatrapur, Odisha, 761020, India*
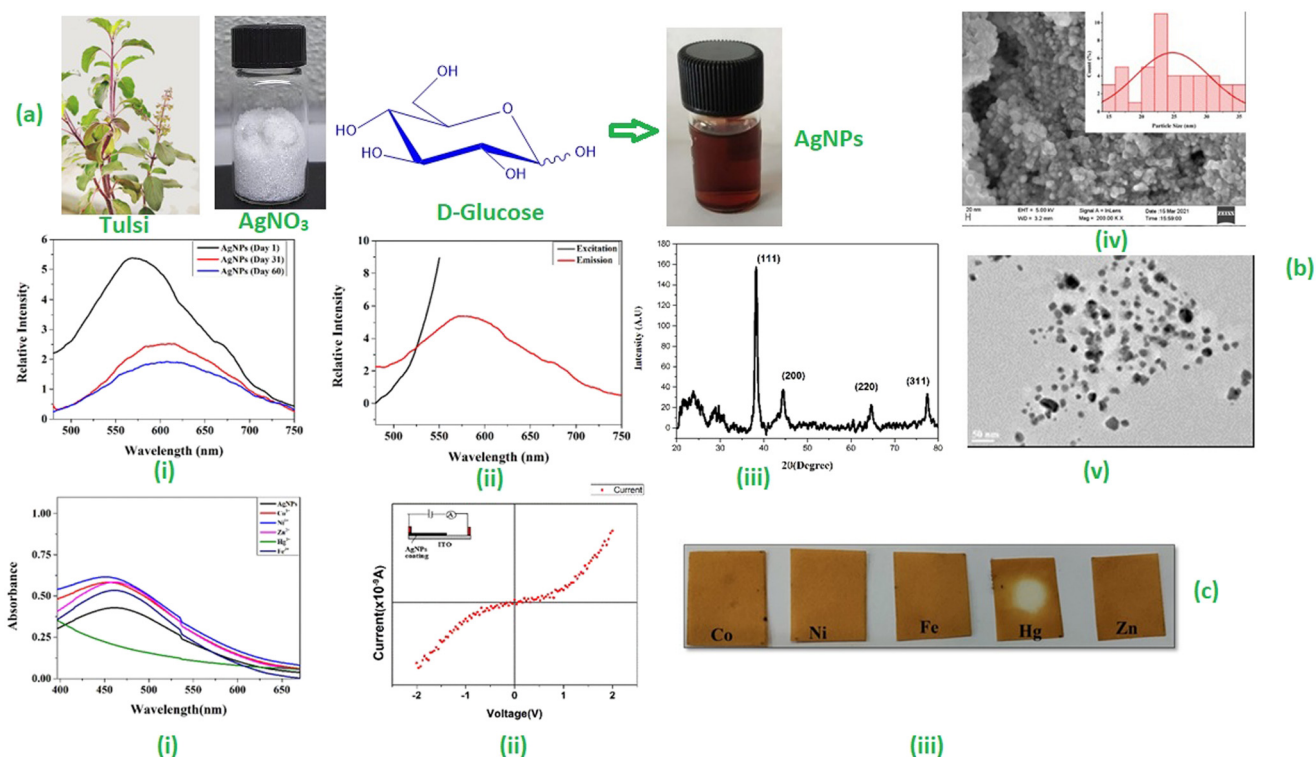
Therefore, monitoring and developing a system to detect the mercury ion level in the environment are essential for protecting humankind from serious health hazards.

Electrothermal atomic absorption spectrometry (ETAAS), cold vapour atomic absorption spectrometry (CVAAS), hydride generation atomic fluorescence spectrometry (HGAFS), and cold vapour atomic fluorescence spectrometry (CVAFS) are the commonly used methods for the detection of mercury, which depend upon the mercury-ligand complex formation.[3,10,11] Since most of these methods are expensive, developing an environment-friendly, cost-effective, quick, and field-applicable detection method with high selectivity and sensitivity is of great interest among researchers. Nanochemistry plays an essential role in detecting this heavy metal ion in the form of a biosensor. Several metal nanoparticles have been used as sensors for $Hg^{2+}$ ions. Among them, the noble metal nanoparticles, mainly silver nanoparticles (AgNPs), are found to be very promising, due to their versatile properties and application in the field of diagnostic medicine,[12] antimicrobial studies, and therapeutics.[13–16] Although there are different chemical methods reported for the synthesis of stable AgNPs, the use of the green method has attracted considerable attention due to its safe synthetic procedures, use of environment-friendly renewable resources, nontoxic solvents, ambient temperature, pressure, *etc.*[17] Plant-mediated green-route synthesized AgNPs

have many advantages compared to chemically synthesized AgNPs. The chemical methods include the use of toxic chemicals as reducing and stabilizing agents, requiring high temperatures. A few methods reported in the literature have used AgNPs as coating materials in designing a sensor for detecting $Hg^{2+}$ ions. Investigations on sensors, based on AgNP coating, have a critical issue, *i.e.*, stability of the nanoparticles, due to which the coating nanomaterial is to be replaced frequently. Therefore, a low-cost and more sensitive sensor design with an environment-friendly coating nanomaterial is the need of the future generation.

In the present work, we used a unique combination of silver salt, tulsi, and commonly available sugar, *i.e.*, D-glucose, for the green synthesis of AgNPs. This method includes the capability of *Ocimum sanctum* leaf extract as a green reducing agent to synthesize AgNPs, which are stabilized by D-glucose used as a capping agent. It was observed that the AgNPs of size 5–45 nm can be synthesized at room temperature without using any specific conditions. The detailed structural analysis was carried out by using different analytical methods. Further, the synthesized nanomaterials were used as coating materials for their applicability as optical sensors for detecting $Hg^{2+}$ ions (Scheme 1). It was found that the LOD of $Hg^{2+}$ ions with glucose-capped AgNPs is 2.8 ppb, compared to the value of 5.3 ppb of its uncapped counterpart.



**Scheme 1** (a) Green synthesis of glucose-capped AgNPs using *Ocimum sanctum* leaf extract. (b) Characterization of synthesized AgNPs: (i) UV-visible spectra indicating the formation of stable AgNPs; (ii) fluorescence spectra of the synthesized AgNPs; (iii) XRD plot confirming the face-centered cubic (fcc) crystalline nature of AgNPs; (iv) SEM image of the AgNPs; and (v) TEM image of the AgNPs. (c) Application of AgNPs: (i) UV-visible spectra showing the interaction of green AgNPs with different transition metal ions; (ii) *I*–*V* characteristic curve of AgNPs; and (iii) visual illustration of the paper strip method of the AgNP-based naked-eye $Hg^{2+}$ sensor showing the change in colour before and after addition of AgNPs.

# 2. Experimental section

## 2.1 Materials and methods

Silver nitrate (99%) and dextrose (α-ᴅ-glucose) of high purity were obtained from Sigma-Aldrich. *Ocimum sanctum* (tulsi) leaves were collected from Berhampur University campus. Deionized water prepared using a Milli-Q water purification system was used throughout the experiments.

## 2.2 Preparation of *Ocimum sanctum* (tulsi) leaf extract

Fresh tulsi leaves (Fig. 1a) were collected and washed several times with distilled water to remove the dust particles. The leaves were finally washed with deionized water and kept for air drying. The dried leaves were cut into fine pieces and crushed with the help of a mortar and pestle. Around 4 g of finely powdered leaves were added to 80 mL of water taken in a 250 mL conical flask and heated at 60 °C for 10 min with constant stirring. The plant extract thus obtained was allowed to cool at room temperature and then filtered using Whatman filter paper to give a brown colour solution (Fig. 1b). This filtrate was stored at 4–8 °C in the refrigerator and used as a reducing agent for the synthesis of AgNPs.

## 2.3 Preparation of an equimolar mixture of glucose and silver nitrate

For the preparation of a silver nitrate solution (10 mmol), 170 mg of silver nitrate was dissolved in 100 mL of deionized water. The sugar solution was prepared by dissolving 18 mg of glucose in deionized water (10 mL) taken in a 100 mL volumetric flask. Then, 10 mL of 10 mmol silver nitrate solution was added to the prepared glucose solution. Deionized water was added to the volumetric flask to make up the volume, giving a 1 : 1 mixture of silver nitrate and glucose. The sugar solution used here acts as a capping and stabilizing agent for the AgNPs.[18]

## 2.4 Synthesis of silver nanoparticles

First, 1 mL of plant extract was added to 9 mL of silver nitrate–glucose solution taken in a 15 mL sample tube. This mixture was shaken well and stirred at room temperature for one hour. The colour of the mixture started changing from yellow to yellowish-brown (Fig. 1c) within 10 minutes which became reddish-brown after one hour, indicating the formation of AgNPs (Fig. 1d).

## 2.5 Design of optical sensors for the detection of Hg$^{2+}$ ions

Fig. 2a illustrates the schematic diagram of the modification of optical fibers for the coating of AgNPs. Modifying the optical fiber is necessary to couple the metal nanoparticles to the surface of the sensing optical fiber. Some specific treatment is required to immobilize nanoparticles on the surface of the fiber. About 30 cm of unclad poly(methyl methacrylate) optical fiber having a diameter of 250 μm was taken, and a 2 cm length from the middle of the fiber was then dipped in a piranha solution (30% $H_2O_2/H_2SO_4$, 7: 3) for 30 minutes. The role of the piranha solution is to provide hydroxyl groups to the surface and also to remove the impurities present on the fiber. The fiber was taken out of the piranha solution and was properly cleaned with deionized water. Then, the probe was soaked into a solution of 3-aminopropyltrimethoxysilane (APTMS) and methanol (1 : 10) for 24 hours, which introduced an amino group with a positive charge on the fiber surface. Due to the electrostatic force,[19] the AgNPs with a negative electric charge get attached to the fiber.[20] At last, the sensing portion was dipped into the prepared AgNPs solution for 24 hours. The fiber was then rinsed with deionized water and dried.

A similar experimental setup was designed for the study of the sensing behaviour of the synthesized AgNPs following our earlier work.[21,22] The setup (Fig. 2b) consists of the light source and the sensing section contains AgNP-coated optical fibers and a detector. Red laser light (630 nm) from the source is passed into the fiber using a source-to-fiber coupler. The signal at the other end of the fiber is received by a
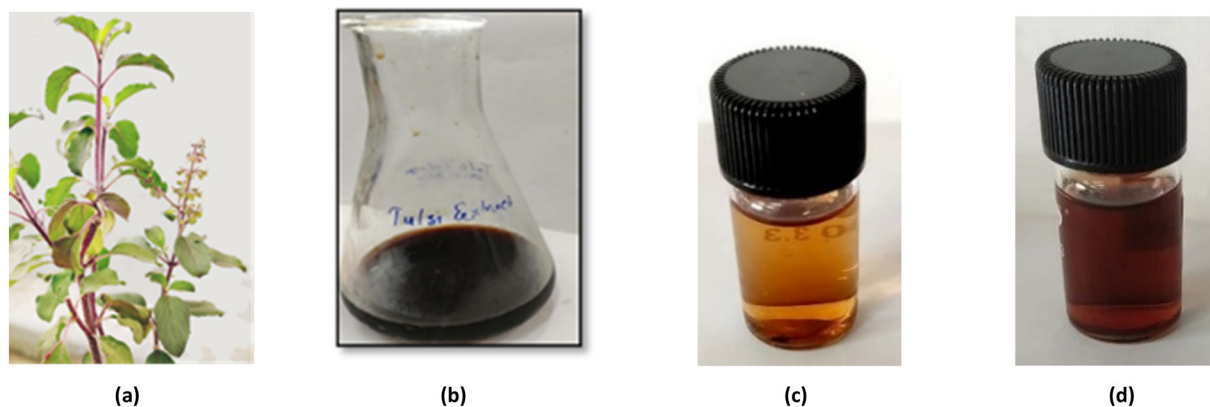


**Fig. 1** (a) *Ocimum sanctum* plant. (b) Aqueous extract of *Ocimum sanctum* leaves. (c) Initial yellowish-brown colour of the mixture. (d) Reddish-brown colour of the mixture after the formation of AgNPs.
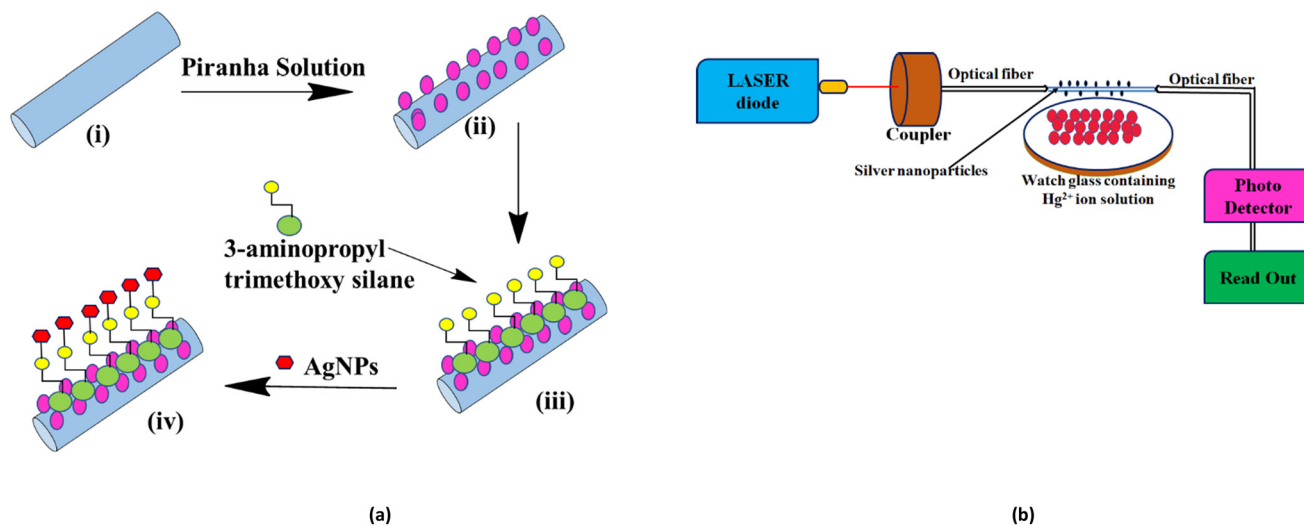
**Fig. 2** (a) Schematic diagram of the AgNPs sensing probe: (i) unclad optical fiber; (ii) hydroxylated fiber surface; (iii) 3-aminopropyl trimethoxy silane group is attached to the fiber on the surface; and (iv) AgNPs are attached on the surface of the fiber by the chemical method. (b) Schematic of the optical fiber sensing experimental system.

detector, which is connected to a measuring unit from which the output power is measured directly by a digital readout. The variation in current in μA was measured with different concentrations of $Hg^{2+}$ by dipping fiber A (AgNPs without sugar) and B (AgNPs capped with sugar).

# 3. Results and discussion

The change in the colour of the AgNPs solution was observed through the naked eye. The colour of the solution changed from colourless to yellowish-brown and, eventually, to reddish-brown, indicating the formation of AgNPs in the solution. The formation of AgNPs was further confirmed by UV-visible, fluorescence spectroscopy, X-ray diffraction (XRD) study, scanning electron microscopy (SEM), and transmission electron microscopy (TEM).

### 3.1 UV-visible absorption analysis

The formation and stability of AgNPs were investigated using a Systronics PC-based double-beam UV-visible spectrophotometer (model-2202). The absorption spectrum of glucose-capped AgNPs solutions was recorded in the wavelength range of 300–700 nm. The UV-visible spectrum (Fig. 3a) showed an absorption maximum at 459 nm, confirming the formation of AgNPs. The stability of the AgNPs dispersed in water was checked at various intervals, *i.e.*, on the 1st, 31st, and 60th days. The characteristic peak corresponding to AgNPs was observed in all cases. These data confirmed that the synthesized AgNPs are stable for at least 60 days in the solution in the presence of sugar, which acts as a capping and stabilizing agent. The interaction of the –OH groups of the D-glucose molecules with the AgNPs probably contributes to the better stability of the glucose-capped AgNPs compared to the uncapped ones.

### 3.2 Fluorescence spectroscopic analysis

The photoluminescence behaviour of AgNPs was observed using an RF-5301PC spectrofluorimeter (Shimadzu). Photoluminescence emission mainly depends on the excitation wavelength of AgNPs (Fig. 3b). It was observed that the emission wavelength was more significant than the excitation wavelength.

The emission spectra were recorded between 450 and 750 nm with a slit-width of 10 mm. Using an excitation wavelength of 450 nm, the photoexcitation of AgNPs produced a very intense emission peak at 577 nm. The fluorescence emission study was performed at different time intervals (Fig. 3c). The results indicated that by increasing time, the concentration increased with the decrease in fluorescent intensity and redshift in the wavelength range from 571 nm to 614 nm.

### 3.3 X-ray diffraction studies

The prepared AgNP solution was centrifuged at 13500 rpm for 30 minutes. The formation of AgNPs was verified using a powerful X-ray diffraction (XRD) tool. The XRD pattern was measured by drop-coated films of AgNPs on a glass plate using an X-ray diffractometer (AXRD benchtop powder diffraction system) ($\lambda = 1.5405$ Å) in the range of 20° to 80° at a scan rate of 0.025° s$^{-1}$. The XRD pattern of AgNPs (Fig. 3d) showed four characteristic peaks having 2θ values of 38.24°, 44.38°, 64.69° and 77.46° corresponding to the (111), (200), (220), and (311) crystalline planes for the face-centered cubic (fcc) crystalline structure of the AgNPs (JCPDS file no. 04-0783). The Debye–Scherrer equation ($D = (k\lambda)/(\beta \cos \theta)$) was used to determine the average crystallite diameter from the half-width of various peaks. The plane (111) having a 2θ value of 38.24° was chosen to calculate the crystallite size. The
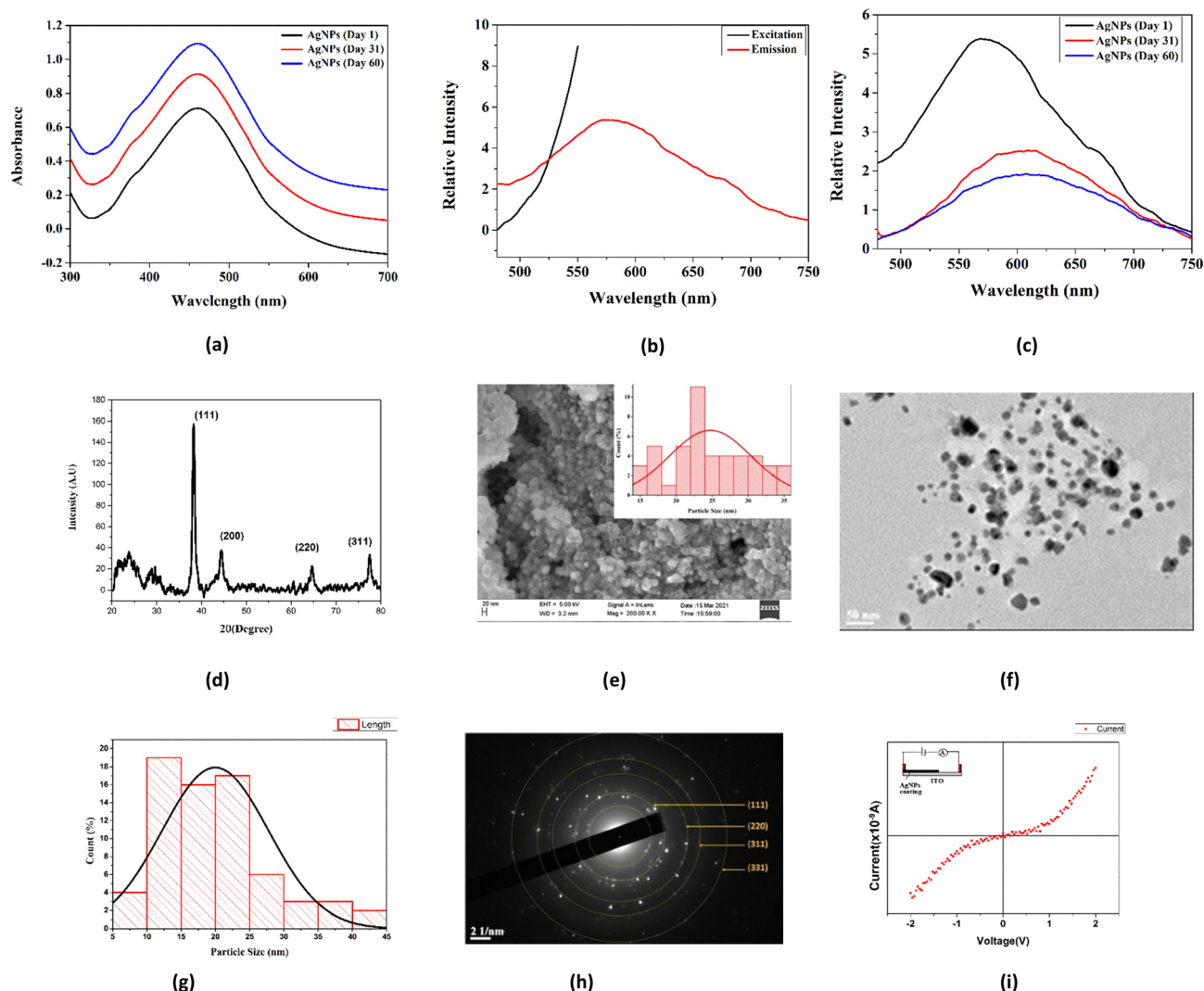
© 2023 The Author(s). Published by the Royal Society of Chemistry

**Fig. 3** (a) UV-visible spectra of glucose-capped AgNPs at different time intervals. (b) Photoluminescence spectra of AgNPs: (i) excitation spectrum and (ii) emission spectrum. (c) Emission spectrum under excitation at 450 nm at different time intervals. (d) X-ray diffraction image of AgNPs. (e) SEM image along with particle size distribution histogram. (f) TEM image. (g) Particle size distribution histogram in TEM. (h) SAED pattern of AgNPs in TEM. (i) *I–V* characteristics curve of AgNPs, the inset figure showing the schematic of an AgNP/ITO junction device.

average crystallite size of synthesized AgNPs was 13.68 nm, and the strain value was approximately 0.00907.

### 3.4 Scanning electron microscopic analysis

The surface morphology of the synthesized AgNPs was further analyzed using a scanning electron microscope. The SEM analysis of the nanoparticles confirmed the spherical nature of AgNPs with an average particle size of 25.74 nm (Fig. 3e). The particle size histogram showed the distribution of particles in the size range of 15–35 nm.

### 3.5 Transmission electron microscopic analysis

The TEM image of synthesized AgNPs showed that the particles were nearly spherical in shape (Fig. 3f). The data from the TEM image were analyzed using the ImageJ software to obtain the average particle size and particle size

distribution histogram. The synthesized nanoparticles were distributed in the size range of 5–45 nm (Fig. 3g). The mean size of 20.08 nm was in good agreement with the particle size calculated from the SEM data. The selected area electron diffraction (SAED) pattern (Fig. 3h) revealed the crystalline nature of the Ag nanostructure. The SAED data showed the diffraction rings with d spacings, which were indexed according to the fcc structure of AgNPs. The concentric rings showed that the synthesized nanoparticles had excellent crystallinity.

### 3.6 Electrical properties of silver nanoparticles

To investigate the electrical conductivity of Ag nanoparticles, an ITO–Ag nanoparticle junction device was fabricated following the procedure reported in the literature.[23] In brief, synthesized AgNPs were drop-cast onto an ITO glass substrate

and dried inside an oven at 80 °C for 30 minutes to form an AgNP/metal junction, which is represented schematically in the inset of Fig. 3i. The *I–V* properties of the said junction were characterized at room temperature using a Keithley source meter. The forward direction corresponds to a positive bias applied to the top metal Ag contact fabricated on the AgNP film and ground connection with the Ag contact fabricated on the ITO substrate. The *I–V* characteristics curve (Fig. 3i) showed the semiconductor behaviour of the thin film of synthesized AgNPs.

### 3.7 Application of AgNPs in sensing $Hg^{2+}$ ions

This section of the study attempted to establish a colorimetric sensing probe for metal ions in an aqueous solution by directly using the green synthesized AgNPs. The interaction between the AgNPs and different metal ions was observed by colorimetric and UV-visible studies. No visible colour change was observed when freshly prepared solutions of transition metal salts such as $Co^{2+}$, $Fe^{3+}$, $Ni^{2+}$, and $Zn^{2+}$ were added to the AgNP solution. However, a remarkable colour change from brown to colourless was noticed when an aqueous solution of $Hg^{2+}$ ion was added to the AgNPs solution. This interaction of $Hg^{2+}$ with AgNPs clearly described the selectivity and specificity of the colorimetric detection. After observing the colorimetric changes, the spectral change of AgNPs with different transition metal ions was monitored by UV-visible spectroscopy. The UV-visible study showed that the absorbance intensity decreased with the complete disappearance of the absorption peak, with the addition of $Hg^{2+}$ salt solution, whereas no significant change was observed in the case of other metal ions (Fig. 4a).

Two plausible mechanisms were proposed to understand the decrease in absorbance upon the interaction of AgNPs with $Hg^{2+}$ ions (Fig. 4b and c).[24] According to the first mechanism, the reduction in absorbance was due to the surface coating of $Hg^{2+}$ ions on AgNPs. The second mechanism suggests the formation of amalgam between $Hg^{2+}$ ions and AgNPs. Amalgamation occurs due to a slight difference in reduction potential values of $Ag^+/Ag$ (0.80 V)

and $Hg^{2+}/Hg$ (0.85 V), which enables the redox reaction between AgNPs and $Hg^{2+}$ ions. It was also reported that amalgam formation took place by combining $Hg^{2+}$ ions with AgNPs, leading to a slight blueshift of absorption peak.[25–27] Although the blueshift in the present case is very small, the change in absorbance at 450 nm ($\lambda_{max}$) was linearly correlated with the concentration of $Hg^{2+}$ ions treated with AgNPs, as shown in Fig. 5a. The limit of detection (LOD) was found to be 7.826 ppb ($y = 0.0015x + 0.0052$, $R^2 = 0.9556$) for the uncapped AgNPs, whereas, for glucose-capped AgNPs, it was 3.429 ppb ($y = 0.00127x + 0.00481$, $R^2 = 0.99123$).

### 3.8 LOD of silver nanoparticles from an optical fiber study

The results obtained using the optical fiber sensing experiment (Fig. 2b) confirmed the higher selectivity of glucose-capped AgNPs towards $Hg^{2+}$ ions than that of its uncapped counterpart.

The variation in current with the concentration for the two cases is shown in Fig. 5b with the range of 10–100 ppb. The limit of detection was found to be 5.3704 ppb for fiber A and 2.873 ppb for fiber B.

Table 1 summarises the comparison of the LOD of different sensors used for the detection of $Hg^{2+}$ ions. In the present case, the LOD value is found to be 2.8 ppb, which is the best sensor in comparison to many other sensors based on AgNPs. This suggests the possibility of a low-cost and effective sensor for the detection of $Hg^{2+}$ ions.

### 3.9 LOD of silver nanoparticles from a filter paper study

For real-time applications, the nanoparticles were impregnated on the filter paper to get an easy-to-use probe for the detection of $Hg^{2+}$ ions.[33,38] This probe provided naked-eye detection for the sensing of $Hg^{2+}$ ions. The results indicated that the colour of the nanoparticle-treated filter paper, which was slightly brown (Fig. 6a), became colourless after the addition of $Hg^{2+}$ ions (Fig. 6b). In the case of other metal ions, no such visible colour change was observed. This showed the selectivity of AgNPs towards the sensing behaviour of $Hg^{2+}$ ions. In the case of $Hg^{2+}$ ions, the lower
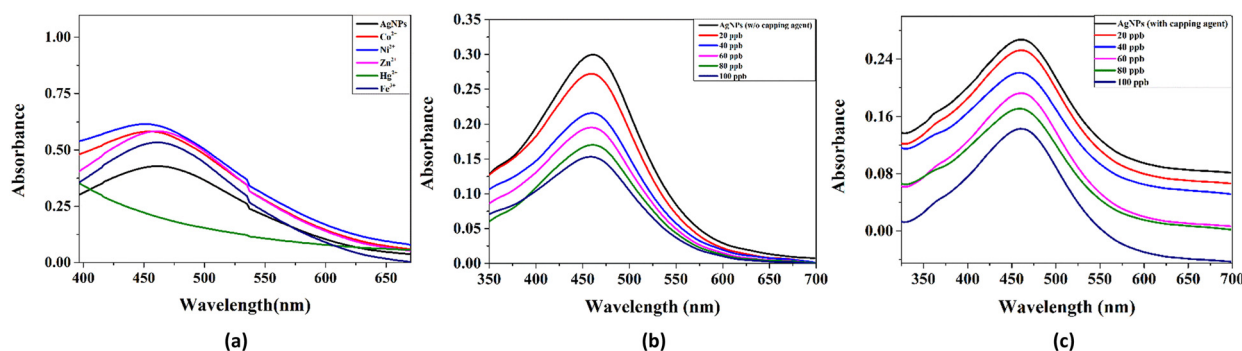


**Fig. 4** (a) UV-visible spectra of green AgNPs with different transition metal ions. (b) UV-visible absorption response of the uncapped AgNP solution upon addition of different concentrations (ppb) of $Hg^{2+}$ ions. (c) UV-visible absorption response of the sugar-capped AgNP solution upon addition of different concentrations (ppb) of $Hg^{2+}$ ions.
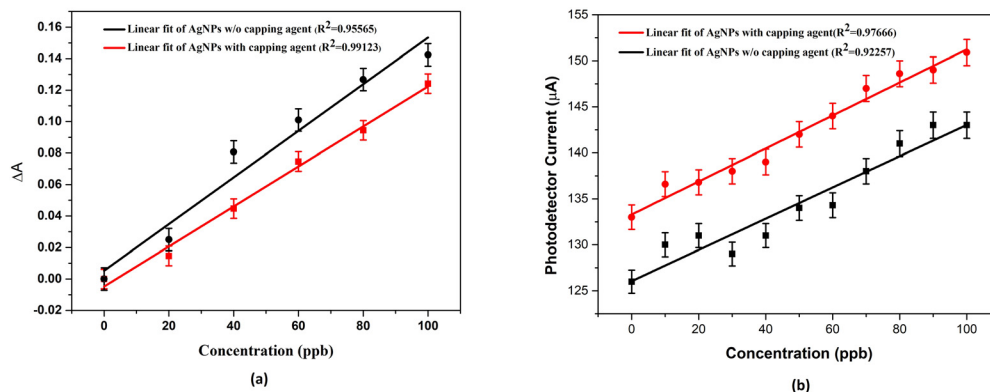
**Fig. 5** (a) Effect of Hg$^{2+}$ ion addition on the absorbance of AgNPs with and without capping agent at 450 nm. (b) Calibration plot of AgNPs with and without sugar for different concentrations of Hg$^{2+}$ (ppb).

**Table 1** Limit of detection (LOD) of different green synthesized silver nanoparticles reported in the literature

| Materials | LOD | Water sample | Reference |
|---|---|---|---|
| AgNPs with starch as a stabilizing agent | 0.12 ppm | Water | 28 |
| AgNPs with *C. cneorum* as a reducing agent | 5 ppb | Water | 29 |
| PVP-AgNPs/printed paper-smartphone | 0.01 ppm | Pond, river, coal mine, and industrial waste | 30 |
| Green silver nanoparticles from *Agaricus bispores* | 0.56 ppm | Lake water | 31 |
| mPEGylated luteolin-functionalized silver nanoparticles | 2 ppm | Tap water | 32 |
| 3-(Trimethoxysilyl) propyl methacrylate functionalized AgNPs | 0.004–0.02 ppm | Water | 33 |
| Green AgNPs with manna of hydras arum plant | 0.42 ppm | Lake water | 34 |
| Green AgNPS with leaf extract of *Mimusops coriacea* | 6.5 ppb | Water | 35 |
| Green AgNPS with *Achillea wilhelmsii* extract | 5.6 ppb | Water | 36 |
| Silver nanoparticles decorated with almond gum molecules | 0.5 ppm | Tap water | 37 |
| Sugar/Tulsi/AgNPs/optical technique | 0.0028 ppm (2.8 ppb) | Water | Present work |



**Fig. 6** Visual illustration of the paper strip method of AgNP-based naked eye Hg$^{2+}$ sensor (a) before adding different metal ion solutions and (b) change in colour after treating with different metal ion solutions.
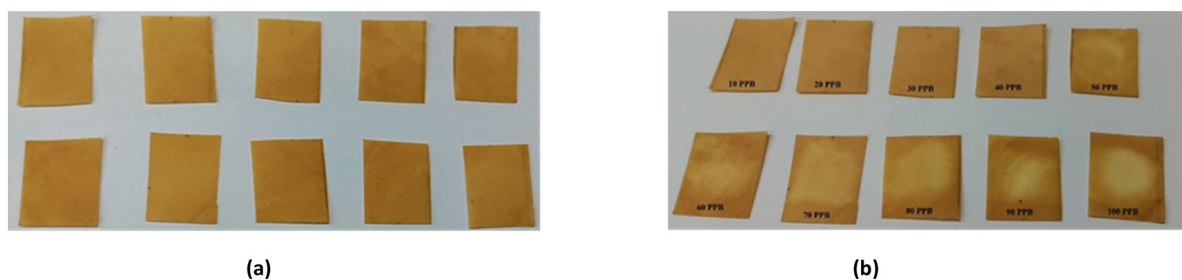


**Fig. 7** Visual illustration of filter papers impregnated with AgNPs (a) before the addition of Hg$^{2+}$ ions and (b) after the addition of different concentrations of Hg$^{2+}$ ions.

limit of sensing of AgNPs was observed when the concentration was about 50 ppb. Fig. 7 represents the photographic image of the prepared probe for the sensing of $Hg^{2+}$ ions.

The decolourization of the probe after the addition of $Hg^{2+}$ ions can be due to the redox reaction between AgNPs and $Hg^{2+}$ ions. $Hg^{2+}$ ions oxidize the AgNPs from $Ag(0)$ to $Ag(\textsc{i})$, leading to decolourization.[28] This explanation was also assisted by a slight blueshift and a decrease in peak intensity in the UV-visible absorption spectra of the solution of AgNPs with the addition of $Hg^{2+}$ ions.

## Conclusions

The present study reported an easy, cost-effective, and green method of synthesizing glucose-capped silver nanoparticles at room temperature. The nanoparticles were characterized by different spectroscopic methods such as UV-visible spectroscopy, fluorescence spectroscopy, XRD, SEM, and TEM. The $Hg^{2+}$ ion sensing applications for the synthesized nanoparticles were investigated using UV-visible and optical studies fabricating two different devices corresponding to the uncapped and capped nanoparticles. The glucose-capped AgNPs were found to be stable for at least two months in an aqueous solution. It was observed that the use of glucose-capped AgNPs as coating materials for sensing applications improved the limit of detection compared to their uncapped counterpart. The limit of detection for $Hg^{2+}$ ions was found to be 2.8 ppb, which showed the best result compared with many other green sensors used for the detection of $Hg^{2+}$ ions. The limit of detection can be improvised by taking other sugar derivatives of different structures for fine-tuning the synthesized green nanoparticles. The results of this investigation can thus be used for the design of low-cost ultrasensitive sensors for the detection of toxic metal ions in aqueous media.

## Author contributions

CP and RM synthesized the silver nanoparticles and did experimental work for the characterization of the nanoparticles. CP and AKS did the optical fiber experiments. LNS helped to analyze, characterize the data, and write the manuscript. NKS helped in the compilation of the data in the manuscript. SKT and SS did the conceptualization, supervision of work, and manuscript writing.

## Conflicts of interest

There are no conflicts of interest to declare.

## Acknowledgements

## References

1 V. K. Gupta, B. Sethi, R. A. Sharma, S. Agarwal and A. Bharti, Mercury selective potentiometric sensor based on low rim functionalized thiacalix[4]-arene as a cationic receptor, *J. Mol. Liq.*, 2013, **177**, 114–118, DOI: **10.1016/j.molliq.2012.10.008**.

2 G. Hilson, Abatement of mercury pollution in the small-scale gold mining industry: Restructuring the policy and research agendas, *Sci. Total Environ.*, 2006, **362**, 1–14, DOI: **10.1016/j.scitotenv.2005.09.065**.

3 Y. Lin, T. Larssen, R. D. Vogt and X. Feng, Identification of fractions of mercury in water, soil and sediment from a typical Hg mining area in Wanshan, Guizhou province, China, *Appl. Geochem.*, 2010, **25**, 60–68, DOI: **10.1016/j.apgeochem.2009.10.001**.

4 F. M. Rebelo and E. D. Caldas, Arsenic, lead, mercury and cadmium: Toxicity, levels in breast milk and the risks for breastfed infants, *Environ. Res.*, 2016, **151**, 671–688, DOI: **10.1016/j.envres.2016.08.027**.

5 Q.-F. Zhang, Y.-W. Li, Z.-H. Liu and Q.-L. Chen, Reproductive toxicity of inorganic mercury exposure in adult zebrafish: histological damage, oxidative stress, and alterations of sex hormone and gene expression in the hypothalamic-pituitary-gonadal axis, *Aquat. Toxicol.*, 2016, **177**, 417–424, DOI: **10.1016/j.aquatox.2016.06.018**.

6 H. H. Harris, I. J. Pickering and G. N. George, The Chemical Form of Mercury in Fish, *Science*, 2003, **301**, 1203, DOI: **10.1126/science.1085941**.

7 M. Harada, Minamata Disease: Methylmercury Poisoning in Japan Caused by Environmental Pollution, *Crit. Rev. Toxicol.*, 1995, **25**, 1–24, DOI: **10.3109/10408449509089885**.

8 P. Grandjean, P. Weihe, R. F. White and F. Debes, Cognitive Performance of Children Prenatally Exposed to "Safe" Levels of Methylmercury, *Environ. Res.*, 1998, **77**, 165–172, DOI: **10.1006/enrs.1997.3804**.

9 C. Salazar-Camacho, M. Salas-Moreno, S. Marrugo-Madrid, R. Paternina-Uribe, J. Marrugo-Negrete and S. Díez, A human health risk assessment of methylmercury, arsenic and metals in a tropical river basin impacted by gold mining in the Colombian Pacific region, *Environ. Res.*, 2022, **212**, 113120, DOI: **10.1016/j.envres.2022.113120**.

10 A. I. Cabañero, C. Carvalho, Y. Madrid, C. Batoréu and C. Cámara, Quantification and Speciation of Mercury and Selenium in Fish Samples of High Consumption in Spain and Portugal, *Biol. Trace Elem. Res.*, 2005, **103**, 17–35, DOI: **10.1385/bter:103:1:017**.

11 P. D. Selid, H. Xu, E. M. Collins, M. S. Face-Collins and J. X. Zhao, Sensing Mercury for Biomedical and Environmental Monitoring, *Sensors*, 2009, **9**, 5446–5459, DOI: **10.3390/s90705446**.

12  S. Schultz, D. R. Smith, J. J. Mock and D. A. Schultz, Single-target molecule detection with nonbleaching multicolor optical immunolabels, *Proc. Natl. Acad. Sci. U. S. A.*, 2000, **97**, 996–1001, DOI: **10.1073/pnas.97.3.996**.

13  M. Rai, A. Yadav and A. Gade, Silver nanoparticles as a new generation of antimicrobials, *Biotechnol. Adv.*, 2009, **27**, 76–83, DOI: **10.1016/j.biotechadv.2008.09.002**.

14  J. L. Elechiguerra, J. L. Burt, J. R. Morones, A. Camacho-Bragado, X. Gao, H. H. Lara and M. J. Yacaman, Interaction of silver nanoparticles with HIV-I, *J. Nanobiotechnol.*, 2005, **3**, 6, DOI: **10.1186/1477-3155-3-6**.

15  N. Jain, P. Jain, D. Rajput and U. K. Patil, Green synthesized plant-based silver nanoparticles: therapeutic prospective for anticancer and antiviral activity, *Micro Nano Syst. Lett.*, 2021, **9**, 5, DOI: **10.1186/s40486-021-00131-6**.

16  S. K. Chandraker, M. Lal, F. Khanam, P. Dhruve, R. P. Singh and R. Shukla, Therapeutic potential of biogenic and optimized silver nanoparticles using *Rubia cordifolia* L. leaf extract, *Sci. Rep.*, 2022, **12**, 8831, DOI: **10.1038/s41598-022-12878-y**.

17  A. Baghizadeh, S. Ranjbar, V. K. Gupta, M. Asif, S. Pourseyedi, M. J. Karimi and R. Mohammadinejad, Green synthesis of silver nanoparticles using seed extract of *Calendula officinalis* in liquid phase, *J. Mol. Liq.*, 2015, **207**, 159–163, DOI: **10.1016/j.molliq.2015.03.029**.

18  E. Filippo, A. Serra, A. Buccolieri and D. Manno, Green synthesis of silver nanoparticles with sucrose and maltose: Morphological and structural characterization, *J. Non-Cryst. Solids*, 2010, **356**, 344–350, DOI: **10.1016/j.jnoncrysol.2009.11.021**.

19  M. Erdmanis, D. Viegas, M. Hautakorpi, S. Novotny, J. L. Santos and H. Ludvigsen, Comprehensive numerical analysis of a surface-plasmon-resonance sensor based on an H-shaped optical fiber, *Opt. Express*, 2011, **19**, 13980–13988, DOI: **10.1364/OE.19.013980**.

20  J. Luo, J. Yao, Y. Lu, W. Ma and X. Zhuang, A Silver Nanoparticle-Modified Evanescent Field Optical Fiber Sensor for Methylene Blue Detection, *Sensors*, 2013, **13**, 3986–3997, DOI: **10.3390/s130303986**.

21  S. P. Dash, S. K. Patnaik and S. K. Tripathy, Investigation of a low cost tapered plastic fiber optic biosensor based on manipulation of colloidal gold nanoparticles, *Opt. Commun.*, 2019, **437**, 388–391, DOI: **10.1016/j.optcom.2018.12.088**.

22  S. K. Swain, G. Phaomei, S. K. Swain, N. K. Sahoo and S. K. Tripathy, A new configuration of fiber optic sensor based on evanescent field absorption utilizing the emission properties of $Fe_3O_4$@$BaMoO_4$: Eu nanocomposite probe, *Opt. Commun.*, 2020, **471**, 125842, DOI: **10.1016/j.optcom.2020.125842**.

23  S. N. Sarangi, B. C. Behera, N. K. Sahoo and S. K. Tripathy, Schottky junction devices by using bio-molecule DNA template-based one dimensional CdS-nanostructures, *Biosens. Bioelectron.*, 2021, **190**, 113402, DOI: **10.1016/j.bios.2021.113402**.

24  S. Manivannan, Y. Seo, D.-K. Kang and K. Kim, Colorimetric and optical Hg(II) ion sensor developed with conjugates of M13-bacteriophage and silver nanoparticles, *New J. Chem.*, 2018, **42**, 20007–20014, DOI: **10.1039/C8NJ04496A**.

25  F. Tanvir, A. Yaqub, S. Tanvir, R. An and W. A. Anderson, Colorimetric Detection of Mercury Ions in Water with Capped Silver Nanoprisms, *Materials*, 2019, **12**, 1533, DOI: **10.3390/ma12091533**.

26  K. Z. Kamali, A. Pandikumar, S. Jayabal, R. Ramaraj, H. N. Lim, B. H. Ong, C. S. D. Bien, Y. Y. Kee and N. M. Huang, Amalgamation based optical and colorimetric sensing of mercury(II) ions with silver@graphene oxide nanocomposite materials, *Microchim. Acta*, 2016, **183**, 369–377, DOI: **10.1007/s00604-015-1658-6**.

27  M. Rex, F. E. Hernandez and A. D. Campiglia, Pushing the Limits of Mercury Sensors with Gold Nanorods, *Anal. Chem.*, 2006, **78**, 445–451, DOI: **10.1021/ac051166r**.

28  A. Apilux, W. Siangproh, N. Praphairaksit and O. Chailapakul, Simple and rapid colorimetric detection of Hg(II) by a paper-based device using silver nanoplates, *Talanta*, 2012, **97**, 388–394, DOI: **10.1016/j.talanta.2012.04.050**.

29  M. Ismail, M. I. Khan, K. Akhtar, J. Seo, M. A. Khan, A. M. Asiri and S. B. Khan, Photosynthesis of silver nanoparticles; naked eye cellulose filter paper dual mechanism sensor for mercury ions and ammonia in aqueous solution, *J. Mater. Sci.: Mater. Electron.*, 2019, **30**, 7367–7383, DOI: **10.1007/s10854-019-01049-x**.

30  Monisha, K. Shrivas, T. Kant, S. Patel, R. Devi, N. S. Dahariya, S. Pervez, M. K. Deb, M. K. Rai and J. Rai, Inkjet-printed paper-based colorimetric sensor coupled with smartphone for determination of mercury ($Hg^{2+}$), *J. Hazard. Mater.*, 2021, **414**, 125440, DOI: **10.1016/j.jhazmat.2021.125440**.

31  M. Sebastian, A. Aravind and B. Mathew, Green Silver Nanoparticles Based Dual Sensor for Toxic Hg (II) Ions, *Nanotechnology*, 2018, **9**, 355502, DOI: **10.1088/1361-6528/aacb9a**.

32  W. Qing, M. Zhao, C. Kou, M. Lu and Y. Wang, Functionalization of silver nanoparticles with mPEGylated luteolin for selective visual detection of $Hg^{2+}$ in water sample, *RSC Adv.*, 2018, **8**, 28843, DOI: **10.1039/C8RA05243C**.

33  S. Balasurya, P. Ahmad, A. M. Thomas, L. L. Raju, A. Das and S. S. Khan, Rapid colorimetric and spectroscopy based sensing of mercury by surface functionalized silver nanoparticles in the presence of tyrosine, *Opt. Commun.*, 2020, **464**, 125512, DOI: **10.1016/j.optcom.2020.125512**.

34  K. Farhadi, M. Forough, R. Molaei, S. Hajizadeh and A. Rafipour, Highly selective $Hg^{2+}$ colorimetric sensor using green synthesized and unmodified silver nanoparticles, *Sens. Actuators, B*, 2012, **161**, 880–885, DOI: **10.1016/j.snb.2011.11.052**.

35  C. R. B. Lopes, D. S. Junior, F. R. de Silva and L. C. Courrol, High-sensitivity $Hg^{2+}$ sensor based on the optical properties of silver nanoparticles synthesized with aqueous leaf extract of *Mimusops coriacea*, *Appl. Phys.*, 2021, **127**, 244, DOI: **10.1007/s00339-021-04391-2**.

36 M. Mavaei, A. Chahardoli, A. Fattahi and A. Khoshroo, A Simple Method for Developing a Hand-Drawn Paper-Based Sensor for Mercury; Using Green Synthesized Silver Nanoparticles and Smartphone as a Hand-Held-Device for Colorimetric Assay, *Global Challenges*, 2021, **5**, 2000099, DOI: **10.1002/gch2.202000099**.

37 S. Y. S. Zeebaree, O. I. Haji, A. Y. S. Zeebaree, D. A. Hussein and E. H. Hanna, Rapid Detection of Mercury Ions Using Sustainable Natural Gum-Based Silver Nanoparticles, *Catalysts*, 2022, **12**, 1464, DOI: **10.3390/catal12111464**.

38 M. L. Firdaus, A. Aprian, N. Meileza, M. Hitsmi, R. Elvia, L. Rahmidar and R. Khaydarov, Smartphone Coupled with a Paper-Based Colorimetric Device for Sensitive and Portable Mercury Ion Sensing, *Chemosensors*, 2019, **7**, 25, DOI: **10.3390/chemosensors7020025**.